Nickel-rhenium compound sheds light on the potency of rhenium as a strengthener in high-temperature nickel alloys

Sascha B. Maisel,[1] Nils Schindzielorz,[1] Alessandro Mottura,[2] Roger C. Reed,[3] and Stefan Müller[1]

[1]*Institute of Advanced Ceramics, Hamburg University of Technology, Denickestrasse 15, Building K, 21073 Hamburg, Germany*
[2]*School of Metallurgy and Materials, University of Birmingham, Edgbaston B15 2TT, United Kingdom*
[3]*Department of Engineering Science, University of Oxford, Oxford OX1 3PJ, United Kingdom*

For many decades, it has been known that rhenium imparts a tremendous resistance to creep to the nickel-based high-temperature alloys colloquially known as superalloys. This effect is so pronounced that is has been dubbed "the rhenium effect." Its origins are ill-understood, even though it is so critical to the performance of these high-temperature alloys. In this paper we show that the currently known phase diagram is inaccurate, and neglects a stoichiometric compound at 20 at.% Re (Ni_4Re). The presence of this precipitate at low temperatures and the short-range ordering of Re in fcc-Ni observed at higher temperatures have important ramifications for the Ni-based superalloys. The Ni_4Re compound is shown to be stable by quantum mechanical high-throughput calculations at 0 K. Monte Carlo simulations show that it is thermally persistent up to $\approx$930 K when considering configurational entropy. The existence of this compound is investigated using extended x-ray absorption fine spectroscopy on a $Ni_{96.62}Re_{3.38}$ alloy.

I. INTRODUCTION

Since the 1980s rhenium has been used as an addition to nickel-based high-temperature superalloys, as even small amounts of rhenium have a dramatic effect on creep resistance [1]. This effect is so pronounced that it is referred to as the *rhenium effect*. The processes underlying the strengthening effect at both high and low temperature are not clearly understood.

Rhenium is so important that generations of Ni-based superalloys are defined upon their rhenium content [2]: First generation alloys have no rhenium, second generation alloys have 2–3 wt.% rhenium, and third generation alloys have 5–6 wt.% rhenium. As an additional element to Ni-based superalloys, rhenium strongly partitions to the γ phase, the single-crystal matrix, where it acts as a potent strengthener. The mechanisms underlying its strengthening effect are still unclear. In the γ phase, rhenium may slow down dislocation glide and/or dislocation climb close to the interfaces between γ and γ' [3], the strengthening precipitates based on $L1_2$-Ni_3Al. This has dramatic effect on the tertiary creep regime observed beyond 1100 K, at stresses below 600 MPa, where dislocations are confined to the γ phase and have to climb around the γ' precipitates in order to contribute to the deformation [2]. It has also been established that rhenium retards the microstructure degradation processes that occur during higher-temperature service [1,4], such as the rafting of γ' precipitates beyond 1250 K. This is attributed to the slow diffusion of rhenium in nickel.

Understanding the distribution of rhenium within the γ phase is paramount to the design of new alloys for high-temperature applications. The current Ni-Re phase diagram [5] suggests that this binary system contains two solid phases, face-centred cubic (fcc) γ-Ni and hexagonal close-packed (hcp) Re. According to the established phase diagram, at typical service temperatures of about 1100 K, up to 8 at.% rhenium is expected to sit in solid solution with Ni in the γ phase. It has been argued that, due to the large miscibility gap, incipient precipitation of Re clusters may be happening at

these Re concentrations, and that solute clustering may explain the abnormal creep strengthening effect of Re additions in the superalloys [6,7]. Since the 1980s, many efforts have focused on determining the distribution of Re in the superalloys, some arguing for the presence of Re clusters [8–10] and some arguing against the presence of Re clusters [11–14].

If Re clusters are present, then these clusters could slow down both dislocation glide and climb during the tertiary creep regimes. These Re clusters, however, would be expected to affect the properties at the low temperature, and it has been shown that Re is a poor strengthener at low temperature [15]. If Re clusters are not present, then Re solute atoms must act alone to slow down the climb of dislocations at the γ/γ' interfaces, and single Re atoms would not pose a barrier to dislocation glide at the typical service temperatures. In this latter case, where the temperature-activated diffusional processes required for climb to happen are retarded by rhenium additions, the presence of short-range ordering may also play an important role.

With this in mind, the Ni-Re system should be revisited, especially considering its importance for transportation and energy production. Is the Ni-Re system immiscible or are there undiscovered intermetallic compounds? Is the Ni-Re solid solution completely disordered or is there short-range ordering of Re in Ni? In this study we use high-throughput density functional theory (DFT) calculations to establish the 0 K convex hull for the Ni-Re binary system. The stability of compounds at finite temperatures is investigated by performing Monte Carlo simulations exploiting cluster expansion (CE) coefficients fitted to a large number of DFT calculations. These predictions are then validated by analyzing extended x-ray absorption fine spectroscopy (EXAFS) data obtained from Ni-Re binary alloys.

II. METHODS

Stable compounds can be discovered by performing a high-throughput search in configuration space. To this end,

an algorithm published by Hart and Forcade [16] exists which is able to exhaustively enumerate all structures on a given lattice and up to a given unit cell size. Using this procedure, face-centered cubic structures with up to 20 basis atoms with a rhenium content of 0–33 at.% Re have been enumerated. This process yields a grand total 213 061 symmetrically inequivalent structures. As it is unfeasible to determine the energy of all 213 061 structures using density functional theory, we have instead evaluated their energies using a cluster-expansion (CE) Hamiltonian [17] fitted to first-principles data.

The CE is a mathematical formalism which represents a quantity that is strictly a function of the atomic arrangement σ on a lattice (like the energy E) as a sum over correlation functions $\overline{\Pi}_F(\sigma)$ times some expansion coefficients J_F. In this case we expand the heat of formation ΔH_{f} for binary structures σ containing x_{Ni} nickel and x_{Re} of rhenium. For this particular problem, the CE expands ΔH_{f} as

$$\Delta H_{\mathrm{f}}(\sigma) = -x_{\mathrm{Ni}}E_{\mathrm{Ni}} - x_{\mathrm{Re}}E_{\mathrm{Re}} + \sum_F J_F\overline{\Pi}_F(\sigma). \qquad (1)$$

The basis functions of the cluster expansion are n-point correlations $\overline{\Pi}_F(\sigma)$, which correspond to different n-body interactions F. The prefactors J_F in the lattice-gas Hamiltonian Eq. (1) can be understood as effective interaction strengths of the respective many-body interactions. In our case, these expansion coefficients J_F are fitted to first-principles free energies, which we have obtained by fully relaxing a structure database of 155 fcc structures. For the relaxation of this first-principles input, the PAW formalism [18] and the generalized gradient approximation as realized in the PW91 potentials [19] supplied with the first-principles code VASP [20,21] have been used. Specifically, the nickel pseudopotential with ten valence electrons as parametrized on 2 August 2007 and the rhenium pseudopotential parametrized on 17 January 2003 with seven valence electrons have been employed. All calculations were performed with full spin polarization. Γ-centered k meshes were used; the k-point sampling has been chosen and tested for each structure individually until absolute convergence with respect to the k mesh was obtained. For integrations within the Brillouin zone, the usual Methfessel-Paxton smearing [22] has been applied.

The energies obtained from these DFT calculations make up the input from which we have constructed the CE Hamiltonians and their effective interaction strengths J_F. The actual fitting of the CE Hamiltonian was performed by a genetic algorithm [23] as implemented in the UNCLE package [24].

III. EXHAUSTIVE GROUND-STATE SEARCHES

Because the CE Hamiltonian [Eq. (1)] can be evaluated very quickly, the energies of all 213 061 structures can readily be determined and plotted into a ground-state diagram (shown in Fig. 1). The system's ground-state compounds lie on the convex hull of that plot (blue line in Fig. 1); it turns out that apart from pure fcc nickel, the binary Ni-Re system exhibits one other extremely dominant ground-state compound at a stoichiometry of Ni₄Re. Its particular configuration is called the $D1_a$ structure (depicted in the inset of Fig. 1) and equivalent to the MoNi₄ prototype [25]. This prototype is clearly unaccounted for in the present Ni-Re phase diagram [5],
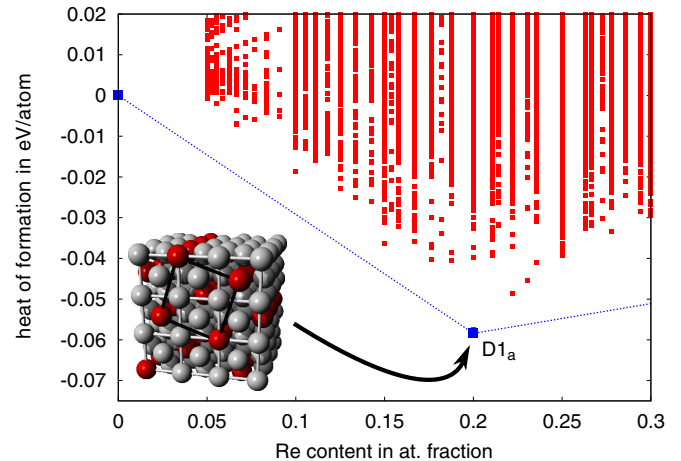

FIG. 1. (Color online) The ground-state diagram for the Ni-Re binary system up to 30% at. rhenium. The ground states lie on the convex hull, which is denoted as a dotted blue line. Sidechart: 3D real-space representation of the $D1_a$ structure with Re atoms depicted in red.

although past first-principles calculations have indicated this structure has a negative heat of formation [26].

It has to be noted that the sizable energy gap between the ground-state structure and all its possible competitors in Fig. 1 is highly uncommon among both Ni-rich systems [27,28] and Re-based alloys [26]. Even systems known to precipitate quite heavily (such as Ni-Al) do not exhibit such a single dominant configuration, but display much more competition in the vicinity of the ground-state line (cf., e.g., the AFLOW data base [29]).

IV. THERMODYNAMIC BEHAVIOR AT ELEVATED TEMPERATURES

So far this analysis only describes the low-temperature behavior of the system, as Fig. 1 is equivalent to the phase diagram at 0 K. However, to incorporate the configurational entropy at finite temperatures, the cluster-expansion Hamiltonian Eq. (1) can be used to drive grand-canonical lattice-gas Monte Carlo simulations to investigate the thermal stability of the Ni₄Re compound and to compute an approximate phase diagram. To this end, a parallel variant [30] of the well-known Metropolis algorithm [31] has been employed to synthesize virtual crystals in a simulated annealing procedure at variable chemical potential $\delta\mu = \mu_{\mathrm{Ni}} - \mu_{\mathrm{Re}}$.

Each crystal contains 50^3 atoms in a cell with face-centered cubic basis vectors. The annealing procedure started at a virtual temperature of $T = 110\,870$ K; this temperature is obviously unphysical, but ensures initially random solute distributions in the Monte Carlo cells. The chemical potentials chosen range from $\delta\mu = -6.44$ to -7.05 eV and the different trajectories resulting from the simulated annealing are shown in Fig. 2. Since grand-canonical ensembles cannot phase separate, the miscibility between pure fcc Ni and the Ni₄Re compound as suggested by the convex hull in Fig. 1 is clearly outlined. The approximate transition temperature can be determined to be $T \approx 930$ K. From the data contained in Fig. 2, it is already
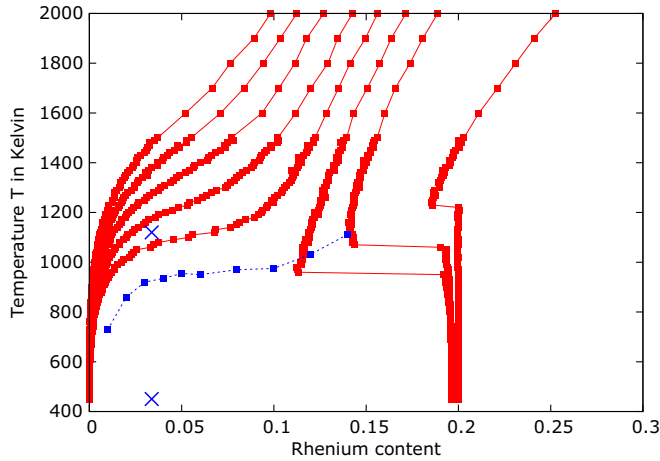
FIG. 2. (Color online) Cooling trajectories of grand-canonical ensembles with different chemical potentials μ. Miscibility gaps appear as large blank areas (e.g., inbetween 20% Re and the dilute solution). The stoichiometric phase to which several of the ensembles are drawn is the Ni_4Re $D1_a$ compound (for details see main text). The phase boundary obtained from canonical ensembles has been superimposed in blue. The two blue crosses are snapshots taken from canonical ensembles shown in Fig. 4.
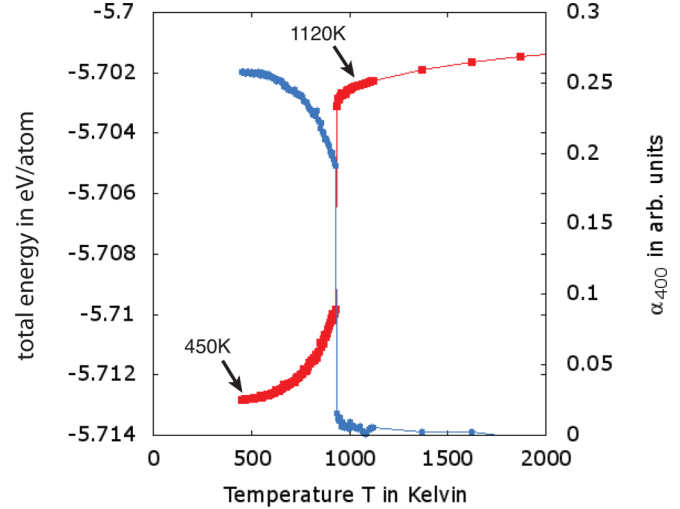

FIG. 3. (Color online) Simulated annealing cooling curve of the total energy (eV/atom) as a function of the temperature as determined from a canonical Monte Carlo cell with $50 \times 50 \times 50$ atoms is shown on the left axis. Cell contains 3.38% Re and 96.62% Ni. The α_{400} ordering parameter is shown on the right axis. A phase transition occurs at 925 K (for details see main text). Note that even above this transition, a tendency for $\langle 400 \rangle$ order remains.

possible to compute an approximate phase diagram. Albeit the Metropolis algorithm only accounts for configurational entropy and thus inherently neglects phononic contributions to the free energy, the contribution of vibrational entropy to the free energy of the $D1_a$ structure was evaluated separately from frozen phonon calculations. This contribution was found to be positive in sign and smaller than 4×10^{-2} eV at 1120 K. Hence, we expect that the vibrational entropy will act to decrease the solvus temperature of the $D1_a$ structure.

To visualize the precipitation process, a canonical ensemble at a fixed Re content of $x_{Re} = 3.38\%$ has been annealed into this miscibility gap; the cooling curve of this canonical ensemble is shown in Fig. 3 (left axis). The Warren-Cowley ordering parameters α_{lmn} (cf. Ref. [32]) governing the crystal can be determined directly from the spatial distribution of atoms in the Monte Carlo cell. These α_{lmn} are a set of parameters defined via the probability $P_{Ni}(Re)_{lmn}$ of finding a Re atom after traveling a vector lmn from a lattice site occupied with a Ni atom. The α_{lmn} are mathematically defined as

$$\alpha_{lmn} = 1 - \frac{P_{Ni}(\mathbf{Re})_{\mathbf{lmn}}}{x_{Re}}. \qquad (2)$$

The coefficient α_{400} is shown in Fig. 3 (right axis); this particular ordering parameter is a quantitative measure for the systems tendency to form $\langle 100 \rangle$ chains [33]. The temperature dependence of $\alpha_{400}(T)$ suggests that: (a) the phase transition at $T \approx 930$ K brings the formation of Re chains with it; and (b) remnant short-ranged order persists above the transition temperature (cf. Fig. 3).

Two sample microstructures ($\langle 100 \rangle$ cuts) produced by this ensemble at temperatures of $T = 450$ and 1370 K (see blue crosses) are shown in Fig. 4. The cut at $T = 1370$ K clearly shows that some ordering mechanism in Ni-Re promotes both the formation of chains and a preferred $\langle 201 \rangle$ Re-Re distance, both of which are characteristic for $D1_a$-type ordering. The

cut at $T = 450$ K shows a precipitate with the expected $D1_a$ atomic structure.

Since the precipitation temperature is relatively low, it is likely that at the operating temperatures of commercial superalloys, these precipitates are dissolved; however some remaining short-range order at elevated temperature, as indicated by Fig. 3, may be present. This remnant short-range order might have a profound impact on the climb of dislocations at the γ/γ' interfaces, by retarding diffusional processes. To quantify the degree of this remaining short-range order, we can simulate the diffuse scattering pattern the virtual Ni_xRe_y crystal would generate in a diffuse scattering experiment under synchrotron radiation. This can be done because the diffuse scattering intensity is proportional to the Fourier transform of the crystals Warren-Cowley parameters. The $\langle 100 \rangle$ cut through the resulting scattering intensities in reciprocal space of the cells can be seen to the right of their respective microstructures in Fig. 4.

Both diffraction patterns can be explained very naturally. The high intensities at the Γ points (corners) of Fig. 4 indicate a phase-separating behavior. This is superposed with intensities near the $\frac{1}{5}\langle 420 \rangle$ and equivalent spots, which are characteristic for $D1_a$-type order [34]; a purely $D1_a$-ordered crystal would generate a diffuse diffraction pattern that consists of δ functions at $\frac{1}{5}\langle 420 \rangle$.

The diffraction pattern at temperatures above the transition temperature does show only minimal intensities at the Γ points, indicating solid solution [cf., e.g., Fig. 4(c)]. While a random alloy would exhibit roughly constant intensities across the entire Brillouin zone, the scattering pattern in Ni-Re features distinct contours. The overall shape is not unlike the ones found in Ni-W [35] or Ni-Mo single crystals [36–38]. From the relative amplitudes of the in the diffractions patterns in Figs. 4(b) and 4(d), we can deduce that the ordering strength
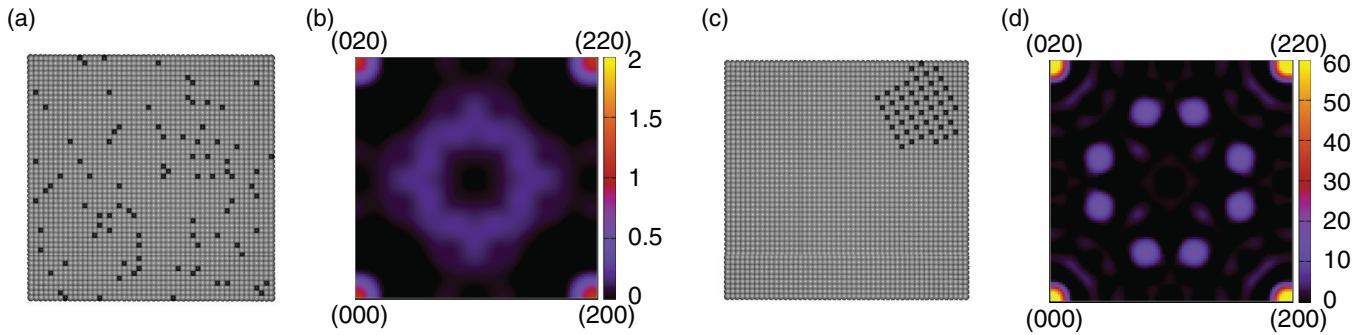
FIG. 4. (Color online) Two (100) cuts through microstructures before [(a) 1120 K] and after [(c) 450 K] the phase transition are shown. At 450 K, precipitation into $D1_a$-ordered precipitates is clearly visible. (b) and (d) The theoretical diffuse scattering intensity calculated from the microstructures (a) and (c), respectively. The superlattice reflections seen in (d) are situated in $\frac{1}{5}\langle 420 \rangle$ and equivalent spots, which are characteristic for $D1_a$-type order. Note: The two scattering patterns have been visualized on different color scales.

drops by about two orders of magnitude, but is still present even above the transition temperature. This is consistent with the sudden decrease of $\alpha_{400}(T)$ to a smaller, yet finite value above the transition temperature (seen in Fig. 3).

V. EXPERIMENTAL CONFIRMATION OF Ni$_4$Re

To validate these predictions, extended x-ray absorption fine spectroscopy (EXAFS) was used to investigate the lattice site occupation and crystal structure surrounding Re atoms in a Ni-Re binary alloy. The oscillations in x-ray absorption coefficient from 20–30 eV to 500–1000 eV beyond the absorption edge of an atom are a consequence of excited photoelectrons being scattered by the surrounding environment. The Fourier transform of the normalized oscillatory part of the x-ray absorption represents a radial distribution of all the possible photoelectron paths. This spectra $\chi(R)$ can be compared to simulated spectra resulting from possible crystal arrangements, obtained from an equation based on single-point scattering theory [39,40].

A 400 g Ni-Re polycrystalline ingot, containing 10 wt.% Re (3.38 at.% Re), was prepared for the EXAFS experiments. The ingot was homogenized by annealing for 7 days in flowing argon at 1523 K and furnace cooled to ambient conditions. The EXAFS data collection was carried out at the Synchrotron Radiation Source (SRS) at Daresbury Laboratory, Warrington, UK. Further detail covering the experimental setup is provided in the Supplemental Material [41] as well as in a previous publication [12]. The Re L_3 edges were measured by three fluorescence scans, the data were cleaned and averaged using Athena [42] and subsequently analyzed using Artemis [42], a front-end graphical interface to the well-known IFEFFIT library [43].

This data were previously analyzed to discern whether hcp-Re or fcc-Re clusters may be present at these concentrations of Re in a Ni-Re binary alloy. The analysis indicated that Re is surrounded by 12 Ni nearest neighbors, suggesting these clusters would not form within the γ phase. Simulating the EXAFS spectra arising from a single Re atom sitting in the fcc-Ni lattice resulted in a satisfactory fit with the EXAFS data, and previous work focused on characterizing the nearest-neighbor shell of atoms. In light of the stability of the $D1_a$-Ni$_4$Re compound up to 930 K, it is important to check whether this would be consistent with the EXAFS data.

The $\chi(R)$ spectra for the Re L_3 edge of the Ni-Re alloy is shown in Fig. 5(a). Simulated $\chi(R)$ spectra for both a Re atom embedded in fcc-Ni and $D1_a$-Ni$_4$Re provide an equally reasonable fit to the experimental data, despite only using the minimum number of parameters (four). The fit arising from hcp-Re (δ) does not match with the EXAFS data, suggesting the alloy does not lie in a two phase field of γ and δ [Fig. 5(a)]. Other structures, predicted by DFT to be close to the Ni-Re convex hull, were also tested and resulted in fits with much higher χ^2 values (see Supplemental Material [41]).

Despite the negligible solid solubility of Re in fcc-Ni predicted by the Monte Carlo simulations, it is expected that some Re will remain in solid solution in fcc-Ni, while the
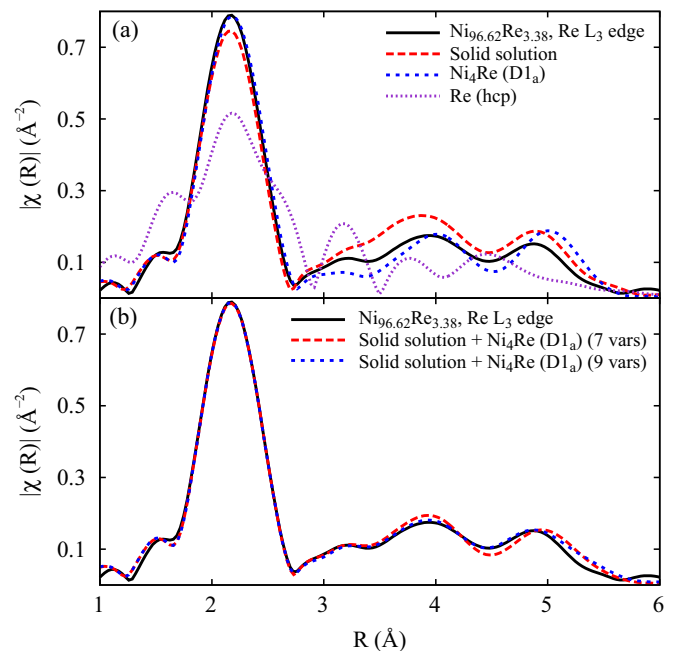

FIG. 5. (Color online) The $|\chi(R)|$ spectrum obtained from the Re $L3$ edge in a binary Ni$_{96.62}$Re$_{3.38}$ alloy compared with (a) simulated spectra for a Ni-Re solid solution, the Ni$_4$Re-$D1_a$ phase and the Re-hcp phase fitted using four EXAFS variables, and (b) simulated spectra for a two phase mixture of Ni-Re solid solution and Ni$_4$Re-$D1_a$ phase fitted using seven and nine EXAFS variables.

rest will either form the $D1_a$-Ni$_4$Re phase or will be part of remnant short-range ordering. Therefore, photoelectron paths from both structures may contribute to the acquired spectra. To test this, paths from both structures were used to fit the EXAFS data [Fig. 5(b)]. In this case, each structure would have an independent set of parameters, except for E_0, common to all photoelectron paths. This brings the total number of fitting parameters to seven, not unreasonable given that the number of independent points for this $\chi(R)$ spectra is ∼18. The resulting fit has an R factor of 0.005, closely replicating the collected data. The relative amplitude for the photoelectron paths arising from a Re in fcc-Ni and $D1_a$-Ni$_4$Re are ≈0.55 and ≈0.45, respectively, suggesting that both sets of photoelectron paths are necessary to produce an adequate fit. It is however important to point out that the relative amplitudes of the photoelectron paths from the two structures are highly correlated. Adding distinct variables to represent the Debye-Waller factor of multiple-vertex scattering paths, bringing the total number of fitting parameters to nine, yields a fit with an R factor of 0.001 [Fig. 5(b)].

VI. SUMMARY

We come to the conclusion that alloying Ni with Re may lead to the formation of $D1_a$-Ni$_4$Re precipitates at lower temperatures. Observations of these precipitates in 1D and 3D atom probe data may be dependent on sample cooling conditions. At elevated temperatures (exceeding 1000 K), these precipitates would dissolve leaving some remnant short-range order of solute atoms which can be seen in both virtual Monte Carlo crystals (cf. Fig. 4) and EXAFS experiments on a Ni$_{96.62}$Re$_{3.38}$ specimen (cf. Fig. 5). This ordering tendency of binary Ni-Re is not accounted for in any of the phase diagrams currently in circulation and may play a role in the anomalous strengthening potency of Re in Ni-rich superalloys by retarding the necessary diffusional processes of dislocation climb. The authors sincerely hope that this work stimulates further research in that regard. It is also likely that future studies of Re diffusion in γ-Ni matrices with strong Ni-Re ordering will reveal some of the previously unexplained features of Re alloying in superalloys—the authors sincerely hope that this work stimulates further research in that regard.

[1] A. F. Giamei and D. L. Anton, Metall. Trans. A **16**, 1997 (1985).

[2] R. Reed, *The Superalloys: Fundamentals and Applications* (Cambridge University Press, Cambridge, 2006).

[3] X.-X. Yu and C.-Y. Wang, Acta Mater. **57**, 5914 (2009).

[4] F. Diologent and P. Caron, Mater. Sci. Eng. A **385**, 245 (2004).

[5] H. Okamoto, J. Phase Equilib. **13**, 335 (1992).

[6] D. Blavette, E. Cadel, and B. Deconihout, Mater. Charact. **44**, 133 (2000).

[7] D. Blavette, E. Cadel, C. Pareige, B. Deconihout, and P. Caron, Microscopy Microanal. **13**, 464 (2007).

[8] D. Blavette, P. Caron, and T. Khan, Scr. Metal. **20**, 1395 (1986).

[9] N. Wanderka and U. Glatzel, Mater. Sci. Eng. A **203**, 69 (1995).

[10] J. Rüsing, N. Wanderka, U. Czubayko, V. Naundorf, D. Mukherji, and J. Rösler, Scr. Mater. **46**, 235 (2002).

[11] P. Warren, A. Cerezo, and G. Smith, Mater. Sci. Eng. A **250**, 88 (1998).

[12] A. Mottura, R. Wu, M. Finnis, and R. Reed, Acta Mater. **56**, 2669 (2008).

[13] A. Mottura, N. Warnken, M. Miller, M. Finnis, and R. Reed, Acta Mater. **58**, 931 (2010).

[14] A. Mottura, M. Finnis, and R. Reed, Acta Mater. **60**, 2866 (2012).

[15] B. Gan and S. Tin, Mater. Sci. Eng. A **527**, 6809 (2010).

[16] G. L. W. Hart and R. W. Forcade, Phys. Rev. B **77**, 224115 (2008).

[17] J. Sanchez, F. Ducastelle, and D. Gratias, Physica A **128**, 334 (1984).

[18] P. E. Blöchl, Phys. Rev. B **50**, 17953 (1994).

[19] J. P. Perdew and Y. Wang, Phys. Rev. B **45**, 13244 (1992).

[20] G. Kresse and J. Furthmller, Comput. Mater. Sci. **6**, 15 (1996).

[21] G. Kresse and D. Joubert, Phys. Rev. B **59**, 1758 (1999).

[22] M. Methfessel and A. T. Paxton, Phys. Rev. B **40**, 3616 (1989).

[23] G. L. W. Hart, V. Blum, M. J. Walorski, and A. Zunger, Nat. Mater. **4**, 391 (2005).

[24] D. Lerch, O. Wieckhorst, G. L. W. Hart, R. W. Forcade, and S. Müller, Model. Simul. Mater. Sci. Eng. **17**, 055003 (2009).

[25] H. Okamoto, J. Phase Equilib. **12**, 703 (1991).

[26] O. Levy, M. Jahntek, R. V. Chepulskii, G. L. W. Hart, and S. Curtarolo, J. Am. Chem. Soc. **133**, 158 (2011).

[27] S. B. Maisel, M. Höfler, and S. Müller, Nature **491**, 740 (2012).

[28] N. Schindzielorz, K. Nowak, S. B. Maisel, and S. Müller, Acta Mater. **75**, 307 (2014).

[29] S. Curtarolo, W. Setyawan, S. Wang, J. Xue, K. Yang, R. H. Taylor, L. J. Nelson, G. L. Hart, S. Sanvito, M. Buongiorno-Nardelli *et al.*, Comput. Mater. Sci. **58**, 227 (2012).

[30] T. Kerscher, S. Müller, Q. Snell, and G. Hart, in *Parallel Distributed Processing Symposium (IPDPS)* (IEEE International, Washington, DC, 2011), pp. 1234–1241.

[31] N. Metropolis, A. W. Rosenbluth, M. N. Rosenbluth, A. H. Teller, and E. Teller, J. Chem. Phys. **21**, 1087 (1953).

[32] J. M. Cowley, Phys. Rev. **77**, 669 (1950).

[33] S. B. Maisel, T. C. Kerscher, and S. Müller, Acta Mater. **60**, 1093 (2012).

[34] S. Das, P. Okamoto, P. Fisher, and G. Thomas, Acta Metal. **21**, 913 (1973).

[35] S. B. Maisel, N. Schindzielorz, S. Müller, H. Reichert, and A. Bosak, J. Appl. Crystallogr. **46**, 1211 (2013).

[36] J. Spruiell and E. Stansbury, J. Phys. Chem. Solids **26**, 811 (1965).

[37] E. Ruedl, P. Delavignette, and S. Amelinckx, Phys. Status Solidi (b) **28**, 305 (1968).

[38] G. V. Tendeloo, Mater. Sci. Eng. **26**, 209 (1976).

[39] D. E. Sayers, F. W. Lytle, and E. A. Stern, *Point Scattering Theory of X-Ray Absorption Fine Structure*, Vol. 13 of Advances in X-Ray Analysis (Plenum, New York, 1970).

[40] D. E. Sayers, E. A. Stern, and F. W. Lytle, Phys. Rev. Lett. **27**, 1204 (1971).

[41] See Supplemental Material at http://link.aps.org/supplemental/10.1103/PhysRevB.90.094110 for EXAFS fits for additional hypothetical Ni-Re structures.

[42] B. Ravel and M. Newville, J. Synchrotron Rad. **12**, 537 (2005).

[43] M. Newville, J. Synchrotron Rad. **8**, 322 (2001).